# Schechter vs. Schechter: Sub-Arcsecond Gravitational Lensing and Inner Halo Profiles

Chung-Pei Ma

Department of Astronomy, University of California at Berkeley, 601 Campbell Hall, Berkeley, CA 94720; cpma@astro.berkeley.edu

#### ABSTRACT

Sub-arcsecond lensing statistics depend sensitively on the inner mass profiles of low-mass objects and the faint-end slopes of the Schechter luminosity function and the Press-Schechter mass function. By requiring the luminosity and mass functions to give consistent predictions for the distribution of image separation below 1", we show that dark matter halos with masses below  $10^{12}M_{\odot}$  cannot have a single type of profile, be it the singular isothermal sphere (SIS) or the shallower "universal" dark matter profile. Instead, consistent results are achieved if we allow a fraction of the halos at a given mass to be luminous with the SIS profile, and the rest to be dark with an inner logarithmic slope shallower than -1.5 to compensate for the steeper faint-end slope of the mass function compared with the luminosity function. We quantify how rapidly the SIS fraction must decrease with decreasing halo mass, thereby providing a statistical measure for the effectiveness of feedback processes on the baryon content in low-mass halos.

Subject headings: galaxies: evolution – galaxies: structure – gravitational lensing

## 1. Introduction

The distribution of the luminosity of galaxies and the distribution of the mass of dark matter halos are well approximated by the Schechter luminosity function (Schechter 1976) and the Press-Schechter mass function (Press & Schechter 1974), respectively. Both functions increase as a power law towards the low luminosity and mass ends, but the mass function increases with a steeper slope than the luminosity function. Low mass halos must therefore contain relatively less luminous baryonic material in comparison with massive halos. Detailed models of galaxy formation have been able to account for this difference by feedback processes such as supernova explosions, stellar winds, and photo-ionizations that suppress the amount of baryons and star formation rates in low mass halos (e.g., Benson et al. 2002; Somerville & Primack 1999; Kaufmann et al 1993).

In this Letter we examine this issue from a different perspective of small-separation strong gravitational lensing. The image separation distribution of lenses below 1" depends sensitively on both the inner mass profile of galactic halos and the faint end slope of the mass and luminosity functions. We compare the traditional approach that models the lenses as SIS and the Schechter luminosity function, with a dark-matter based approach that models the lenses with a certain halo mass profile and the Press-Schechter mass function. We investigate the constraints on the inner total mass profiles of halos by requiring the two approaches to give consistent predictions. Since evidence based on stellar dynamics of elliptical galaxies (e.g., Rix et al. 1997; Romanowsky & Kochanek 1999; Treu & Koopmans 2002), modeling of lensed systems (e.g., Cohn et al. 2001), and flux ratios of multiple images (Rusin & Ma 2001; Rusin 2002) all give an inner profile for lensing galaxies that is consistent with SIS, we will use SIS in the lensing calculation with the luminosity function. Dark matter halos then clearly cannot all be SIS because if so, the mass function is steeper than the luminosity function and would lead to a relatively higher lensing rate at smaller angular scale. We will show that modifying the SIS to any *single* flatter profile for halos does not work either. Instead, we discuss in  $\S$  4 how a combination of profiles is needed to resolve the problem.

This paper complements several recent studies on strong lensing statistics in which the emphasis is on the effects of lens mass profiles and baryon compression on the cumulative lensing rates at  $\theta \gtrsim 1''$  and the implications for cosmological parameters from the scarcity of large separation ( $\gtrsim 3''$ ) systems (Keeton & Madau 2001; Keeton 2001; Kochanek & White 2001; Kochanek 2001; Sarbu, Rusin, & Ma 2001; Li & Ostriker 2002; Oguri 2002). It is pointed out that modeling cluster-scale lenses with mass profiles shallower than the SIS greatly reduces the lensing rate and brings the concordance CDM model predictions into agreement with observations. The focus here is on the less explored sub-arcsec range. We use the predicted shape for the differential distribution of image separation to quantify how rapidly the fraction of SIS halos must decrease with decreasing mass.

In this paper the cosmological model is taken to have a present-day matter density  $\Omega_m = 0.3$  (with 0.05 in baryons), cosmological constant  $\Omega_{\Lambda} = 0.7$ , Hubble parameter h = 0.75, and matter fluctuation  $\sigma_8 = 0.92$ . The lens potentials are assumed to be spherically symmetric because we are mainly concerned with the lensing optical depth, which is more sensitive to the velocity dispersion and the radial profile of the lens than its ellipticity (Kochanek & Blandford 1987). The luminosity function is assumed to have a constant comoving galaxy number density, which is consistent with the nearly constant comoving halo number density (for a fixed velocity) up to redshift  $\sim 5$  in the Press-Schechter formula (Bullock et al. 2001).

# 2. Lensing Rates from Luminosity and Velocity Functions

The galaxy luminosity function takes the form (Schechter 1976)

$$\phi(L)dL = \phi_* \left(\frac{L}{L_*}\right)^{\alpha} e^{-L/L_*} d\left(\frac{L}{L_*}\right). \tag{1}$$

An alternative measure is given by the (circular) velocity function

$$\psi(v)dv = \psi_* \left(\frac{v}{v_*}\right)^{\beta} e^{-(v/v_*)^n} d\left(\frac{v}{v_*}\right), \tag{2}$$

which is related to the luminosity function by  $L \propto v^n$ ,  $\beta + 1 = n(\alpha + 1)$ , and  $\psi_* = n\phi_*$ . The velocity function can be derived from galaxy survey luminosity functions and kinematic luminosity-velocity relations, e.g., from various large pre-SDSS optical surveys (Gonzalez et al. 2000) and the 2MASS infrared survey (Kochanek 2001). The image separation distribution of lenses at angle  $\theta$  is related to the galaxy velocity function by

$$\frac{dP}{d\theta} = \int dz_l \frac{dr}{dz_l} \frac{dv_c}{d\theta} \,\psi(v_c, z_l) \,\sigma_{\text{lens}}(v_c, z_l) \,B\,, \tag{3}$$

where  $dr/dz = cH_0^{-1}(1+z)^{-1}[\Omega_m(1+z)^3 + \Omega_{\Lambda}]^{-1/2}$  (for  $\Omega_m + \Omega_{\Lambda} = 1$ ),  $\sigma_{\text{lens}}$  is the lensing cross section, B is the magnification bias, and  $\psi(v_c, z_l)dv_c$  is the physical number density of galaxies with circular velocity between  $v_c$  and  $v_c + dv_c$  at lens redshift  $z_l$ .

An SIS lens has a density profile  $\rho(r) = v_c^2/(8\pi G r^2)$  and produces an image separation of  $\theta = 2\theta_E$  where  $\theta_E = 2\pi (v_c/c)^2 D_{ls}/D_s$  is the Einstein radius. For  $\theta = 1''$  and source redshift  $z_s = 1.2$ ,  $v_c$  ranges from 225 to 325 km/s for  $z_l = 0.3$  to 0.7. The lensing cross section is  $\sigma_{\text{lens}} = \pi (\theta_E D_l)^2 = 4\pi^3 (v_c/c)^4 (D_l D_{ls}/D_s)^2$  (Schneider, Ehlers & Falco 1992). For small  $\theta$  (< 1"), one can show analytically that the slope of  $dP/d\theta$  in eq. (3) depends only on the faint-end slope  $\beta$  of the velocity function:

$$\frac{dP}{d\theta} \propto \theta^{(\beta+3)/2} \propto \theta^{n(\alpha+1)/2+1}$$
, for small  $\theta$ , (4)

where  $\beta+1=n(\alpha+1)$  is used to relate  $\beta$  to the faint-end slope  $\alpha$  of the luminosity function and the luminosity-velocity relation  $L \propto v^n$ . The distribution  $dP/d\theta$  therefore has a positive slope on sub-arcsec scale if the velocity function is shallower than  $\beta=-3$ , or if the luminosity function is shallower than  $\alpha=-(1+2/n)$ . Fig. 1 illustrates this dependence. Recent surveys favor  $\beta \sim -1.3$  to -1.0 (e.g., Gonzalez et al. 2000; Kochanek 2001), indicating a positive slope for  $dP/d\theta$  at small  $\theta$ . The image separation distribution of 13 lenses found in the 8958 CLASS radio sources (Browne et al. 2002) is shown in Fig. 1 for comparison. Note that the smallest and largest  $\theta$  bins contain only one lens each.

## 3. Lensing Rates from Mass Functions

Lensing probes mass after all, so let us take an alternative approach by modeling the lenses as a population of dark matter halos with a Press-Schechter type of mass function. Similar to eq. (3), the image separation distribution is given by

$$\frac{dP}{d\theta} = \int dz_l \frac{dr}{dz_l} \frac{dM}{d\theta} n(M, z_l) \,\sigma_{\text{lens}}(M, z_l) \,B, \qquad (5)$$

where  $n(M, z_l)dM$  is the physical number density of dark halos with mass between M and M + dM at  $z_l$ . We use the improved version of the mass function by Jenkins et al. (2001). Unlike the lensing galaxies in eq. (3), the lensing halos in eq. (5) may or may not host central baryons depending on if the lens is baryon or dark matter dominated near its center. We will therefore consider different inner mass profiles. For luminous lenses in which baryon dissipation controls the inner density, we use the SIS profile as in § 2. For dark lenses without a significant amount of baryons, we consider the shallower profiles found in high resolution dark matter simulations:  $\rho \propto r^{-1}$  (Navarro et al. 1997) and  $r^{-1.5}$  (Moore et al. 1999).

The lensing properties of the three profiles – SIS, NFW, and Moore – are as follows. For SIS, we relate the circular velocity  $v_c$  of galaxies to the virial velocity  $v_{vir}$  of dark halos by  $v_c = \gamma_v v_{vir}$ , where  $\gamma_v \sim 1.3$  to 1.8 from various baryon compression models and observational constraints (Oguri 2002 and references therein). We take Oguri's best fit value  $\gamma_v = 1.67$  here. Using  $v_{vir} = (4\pi G^3 M^2 \bar{\rho} \Delta_{vir}/3)^{1/6}$ , we then have  $\theta = AM^{2/3}$  where  $A = 4\pi G(\gamma_v/c)^2 (D_{ls}/D_s)(4\pi \bar{\rho} \Delta_{vir}/3)^{1/3}$  and  $\Delta_{vir} \approx 178$ .

For the Moore et al. profile  $\rho(x) = \bar{\rho} \, \bar{\delta}/(x^{3/2} + x^3)$ , we find the projected surface density  $\Sigma$  well approximated by  $\kappa(x) = \Sigma/\Sigma_c = 5.4\kappa_0/[x^{1/2}(1+1.8\,x)^{3/2}]$  where  $x = r/r_s$ . Here  $\kappa$  is the convergence,  $\Sigma_c = (c^2/4\pi G)(D_s/D_lD_{ls})$  is the critical surface density, and  $\kappa_0 = r_s \bar{\rho} \, \bar{\delta}/\Sigma_c$ . The scale radius  $r_s$  is related to the concentration parameter by  $c \equiv r_{vir}/r_s$ , where  $r_{vir}$  is the halo virial radius, and  $\bar{\delta} = 100\,c^3/\ln(1+c^{3/2})$ . The reduced deflection angle, related to  $\kappa$  by  $\alpha(x) = 2x^{-1}\int_0^x dy\,y\kappa(y)$ , then has the simple analytic form  $\alpha(x) = (12\kappa_0/\sqrt{b}\,x)[\ln(\sqrt{bx}+\sqrt{1+bx})-\sqrt{bx}/\sqrt{1+bx}]$ , where b=1.8. The lensing cross section is  $\sigma_{\rm lens} = \pi(\beta_{rad}D_l)^2$ , where  $\beta_{rad}$  is the angular size of the radial caustic, which we obtain by solving the lens equation.

For the Moore profile, we find the fitting function  $(\beta_{rad}D_l) = 9.3r_s\kappa_0^2/(1-1.1\kappa_0^{0.4}+4.5\kappa_0^{0.9})$  accurate (with < 5% error for  $\kappa_0 \lesssim 6$ ) and useful in speeding up the computation. Since the angular separation of the outermost images is insensitive to the location of the source (Schneider et al. 1992), we use the size of the tangential critical curve for the image separation:  $\theta = 2\theta_{tan}$ . We find the fitting function  $(\theta_{tan}D_l) = 38r_s\kappa_0^2/(1-1.8\kappa_0^{0.6}+19\kappa_0^{1.25})$  accurate (with < 4% error for  $\kappa_0 \lesssim 6$ ). Similarly for the NFW lenses, we use  $(\beta_{rad}D_l) =$ 

$$-4r_s\kappa_0(1-0.4\kappa_0^{0.1}+0.5\kappa_0^{0.2})/\exp[(3+\kappa_0^{-1})/2]$$
 for  $\sigma_{lens}=\pi(\beta_{rad}D_l)^2$ , and  $(\theta_{tan}D_l)=2r_s(1-0.7\kappa_0^{0.5}+1.35\kappa_0^{0.85})/\exp[(1+\kappa_0^{-1})/2]$  for  $\theta=2\theta_{tan}$ .

We compute the magnification bias B from the fitting formula given by eq. (21) in Oguri et al. (2002). We have tested this formula against numerical calculations and found good agreement. A similar fit given by eq. (67) in Li & Ostriker (2002), however, substantially underestimates the bias for  $\kappa_0 \lesssim 1$  and overestimates it for  $\kappa_0 \gtrsim 1$ . This is because their fit assumed  $d\alpha/dx = 0$  and therefore neglected a factor containing  $(1 - d\alpha/dx)$ , where  $\alpha$  is the deflection angle. We find this not to be a valid assumption in general.

Fig. 2 compares  $dP/d\theta$  for SIS, Moore, and NFW lenses computed from the halo mass function in eq. (5), and  $dP/d\theta$  for SIS lenses computed with velocity functions of different slope  $\beta$  in eq. (3). It shows that no single mass profile with the halo mass function can match the  $dP/d\theta$  predicted by the observed velocity function of  $\beta \sim -1.3$ . The SIS (solid) and Moore (long-dashed) profiles predict wrong shapes for  $dP/d\theta$ , a reflection of the steeper faint end of the mass function compared with the luminosity function. The shape of  $dP/d\theta$  for the shallower NFW profile (short-dashed) resembles more closely the velocity function prediction, but the lensing amplitude is miniscule. We note that the magnification bias B has been included in Fig. 2, which is generally significantly higher for shallower inner mass profiles, but the resulting NFW lensing amplitude is still much too low.

## 4. Mass vs. Light: Resolution

To bring the predicted shape for the image separation distribution from eq. (5) into agreement with eq. (3), we explore the possibility that at a given mass, a fraction of the lenses is luminous, baryon dominated at the center and has the SIS profile, while the rest of the lenses is dark matter dominated and has a shallower inner profile. Instead of this bimodal model, one can presumably allow the slope of the inner mass profile to decrease smoothly with mass. Observations of lensing galaxies, however, consistently find that the combined stellar and dark matter mass profile inside the Einstein radius is well fit by the SIS (e.g., Rix et al. 1997; Romanowsky & Kochanek 1999; Cohn et al. 2001; Treu & Koopmans 2002). At the same time, galaxy formation models show that the energetics of feedback processes are sufficient to expel baryons in some  $< 10^{12} M_{\odot}$  halos. The bimodal model combining SIS and dark matter profiles therefore appears physically motivated and will be used below.

From the solid and long-dashed curves in Fig. 2, we conclude that a combination of SIS and Moore profiles cannot reproduce the shape of  $dP/d\theta$  predicted by the velocity function with  $\beta \sim -1.3$ . This is because the inner slope of the Moore profile is close enough to SIS

that the two predict similar shapes for  $dP/d\theta$ . Making some lenses dark with  $r^{-1.5}$  inner profile will therefore not reproduce the monotonically rising  $dP/d\theta$  at small  $\theta$  for the velocity function. If halos have the shallower  $r^{-1}$  profile, however, the dark lenses will have negligible lensing optical depth compared with the SIS (short-dashed vs. solid in Fig. 2). We can then match the two predictions by parameterizing the fraction of SIS halos at a given mass with

$$f_{SIS}(M) \propto \frac{(M/M_c)^{\eta_1 + \eta_2}}{e^{(M/M_c)^{\eta_2}} - 1},$$
 (6)

which grows as a power law,  $f_{SIS} \sim (M/M_c)^{\eta_1}$ , at small M and falls exponentially at large M. This makes the halos mostly SIS on galactic mass scale  $M_c$  where baryon dissipation is important, and mostly NFW on cluster and sub-galactic scales where dark matter dominates the potential. Our main interest here is in determining the slope  $\eta_1$ , which has the convenient property that it depends only on the faint end slope  $\beta$  and not on other parameters in the velocity function in eq. (2). It also gives a simple parameterization of the importance of feedback processes on the density profile as a function of halo mass. We note that since the relation between the image separation  $\theta$  and halo mass M is redshift-dependent, the factor  $f_{SIS}$  must be included inside the integral of eq. (5). We do not consider explicit redshift dependence in  $f_{SIS}$  here, which can be put in at the expense of introducing more parameters. Future work combining  $f_{SIS}$  determined from lensing with galaxy formation models and simulations may offer useful constraints on the time evolution of  $f_{SIS}$ .

Fig. 3 shows the excellent agreement between the two predictions for the shape of  $dP/d\theta$  for four faint-end slopes of the velocity function. The required  $\eta_1$  in eq. (6) is  $\approx 0.85$ , 0.75, 0.53, and 0.2 for  $\beta = -1, -1.3, -2$ , and -3, respectively. The other two parameters  $M_c$  and  $\eta_2$  depend on the shape of the velocity function. For  $v_* = 250$  km s<sup>-1</sup> and n = 2.5 from the SSRS2 sample (Gonzalez et al. 2000), we find a good match with  $M_c \approx 4.5 \times 10^{11} M_{\odot}$  and  $\eta_2 \approx 0.72$ . We also find it necessary to lower the overall amplitude of  $dP/d\theta$  for the dashed curves in Fig. 3 by  $\sim 20\%$  to 40% (for normalized  $f_{SIS}$  shown in Fig. 4) to match the dotted curves. We have not attempted to fine tune it since the amplitude of  $dP/d\theta$  depends on several uncertain parameters, e.g., the source redshift distribution, the normalization and redshift evolution of the luminosity function, and the precise value of  $\gamma_v = v_c/v_{vir}$  for SIS halos. Instead we have focused on the constraints from the shape of  $dP/d\theta$ .

Fig. 4 shows the required  $f_{SIS}(M)$  for each of the four velocity functions in Fig. 3. Our  $f_{SIS}$  at the high mass end for  $\beta = -1.3$  agrees well with the result from Oguri (2002), which used  $f_{SIS}(M) = \exp[1 - (M/M_h)^{\delta_h}]$  for  $M > M_h$  following Kochanek (2001), and set  $f_{SIS} = 1$  for  $M < M_h$ , i.e., it ignored the dark lens fraction for small masses. By contrast, our form of  $f_{SIS}$  in eq. (6) is a smooth function and takes into account all masses.

Fig. 4 illustrates that a very steep faint-end slope ( $\beta \sim -4$ ) for the velocity function will

be required if low-mass halos all have the SIS profile. Current galaxy surveys favor a much shallower faint end slope of  $\beta \sim -1.3$ . We thus conclude that the percentage of halos that can have the SIS profile must decrease rapidly with decreasing halo mass below  $10^{12} M_{\odot}$ . This implies that feedback processes are increasingly effective in reducing the baryon content in small objects, a trend consistent with semi-analytic galaxy formation models. Moreover, the halos that have non-SIS profiles must have an inner density of  $\rho \sim r^{-1}$  or shallower so as to contribute negligible lensing optical depth. (The possibly shallow profiles of dwarf galaxies will therefore not affect the lensing predictions here.) The steeper  $\rho \sim r^{-1.5}$  would predict a shape for the lensing image separation different from the observed luminosity function.

I have enjoyed discussions with Paul Schechter, Joe Silk, Aveshi Dekel, David Rusin, Dragan Huterer, and David Hogg. This work is supported in part by an Alfred P. Sloan Foundation Fellowship, a Cottrell Scholars Award from the Research Corporation, and NASA grant NAG 5-12173.

## REFERENCES

Benson, A. J., Lacey, C. G., Baugh, C. M., Cole, S., & Frenk, C. S. 2002, MNRAS, 333, 156

Browne, I. W. A. et al. 2002, astro-ph/0211069

Bullock, J. S., Dekel, A., Primack, J. R., & Somerville, R. S. 2001, ApJ, 550, 21

Cohn, J. D., Kochanek, C. S., McLeod, B. A., Keeton, C. R. 2001, ApJ, 554, 1216

Gonzalez, A. H., Williams, K., Bullock, J., Kolatt, T., & Primack, J. 2000, ApJ, 528, 145

Jenkins, A. et al. 2001, MNRAS, 321, 372

Kauffman, G., White, S. D. M., & Guiderdoni, B. 1993, MNRAS, 264, 201

Keeton, C. 2001, ApJ, 561, 46

Keeton, C., & Madau, P. 2001, ApJ, 549, L25

Kochanek, C. S. 2001, astro-ph/0108160

Kochanek, C. S., & Blandford, R. D. 1987, ApJ, 321, 676

Kochanek, C. S., & White, M. 2001, ApJ, 559, 531

Li, L.-X., & Ostriker, J. P. 2002, ApJ, 566, 652

Moore, B., Quinn, T., Governato, F., Stadel, J., & Lake, G. 1999, MNRAS, 310, 1147

Navarro, J. F., Frenk, C. S., & White, S. D. M. 1997, ApJ, 490, 493

Oguri, M. 2002, astro-ph/0207520

Oguri, M., Taruya, A., Suto, Y., Turner, E. L. 2002, ApJ, 568, 488

Press, W. H., & Schechter, P. 1974, ApJ, 187, 425

Rix, H.-W., de Zeeuw, P.T., Cretton, N., van der Marel, R.P., Carollo, C. 1997, ApJ, 488, 702

Romanowsky, A. J., & Kochanek, C. S. 1999, ApJ, 516, 18

Rusin, D. 2002, ApJ, 572, 705

Rusin, D., & Ma, C.-P. 2001, ApJ, 549, L33

Sarbu, N., Rusin, D., & Ma, C.-P. 2002, ApJ, 561, L147

Schechter, P. 1976, ApJ, 203, 297

Schneider, P., Ehlers, J., & Falco, E. E. 1992, Gravitational Lenses (Berlin: Springer-Verlag)

Somerville, R. S., & Primack, J. R. 1999, MNRAS, 310, 1087

Treu, T., & Koopmans, L. V. E. 2002, ApJ, 575, 87

This preprint was prepared with the AAS LATEX macros v5.0.

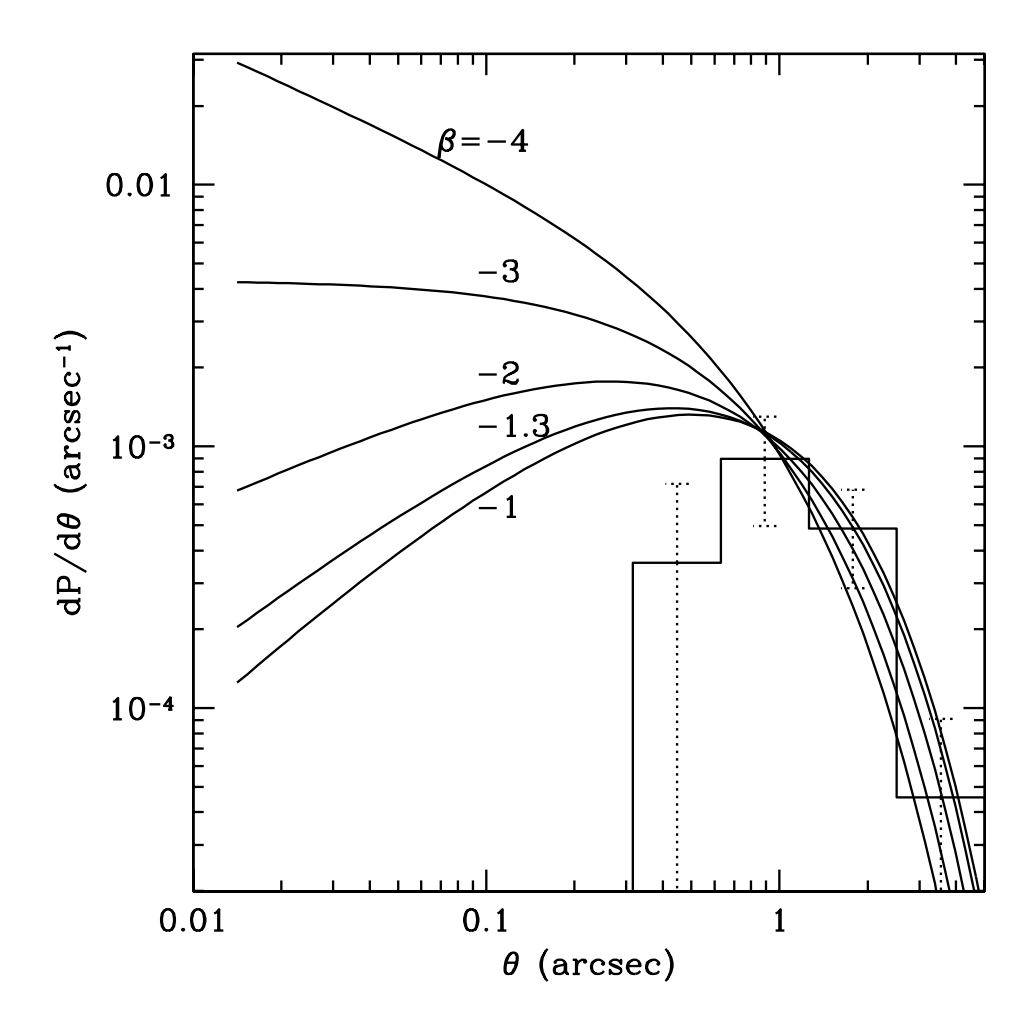


Fig. 1.— Image separation distribution  $dP/d\theta$  calculated from eq. (3) using the galaxy velocity function in eq. (2) and SIS profile. For small  $\theta$ , the slope of  $dP/d\theta$  only depends on the faint-end slope  $\beta$  of the velocity function, changing from positive to negative when the velocity function steepens beyond  $\beta = -3$ . Other velocity function parameters used here are  $v_* = 250 \text{ km s}^{-1}$ , n = 2.5,  $\psi_* = 0.073h^3 \text{ Mpc}^{-3}$  from the SSRS2 sample in Gonzalez et al. (2000). The sources are put at the mean redshift 1.27 of the CLASS radio sources with a power-law flux distribution of slope -2.1. The histogram shows the 13 CLASS lenses and the  $1\sigma$  poisson errors (Browne et al. 2002).

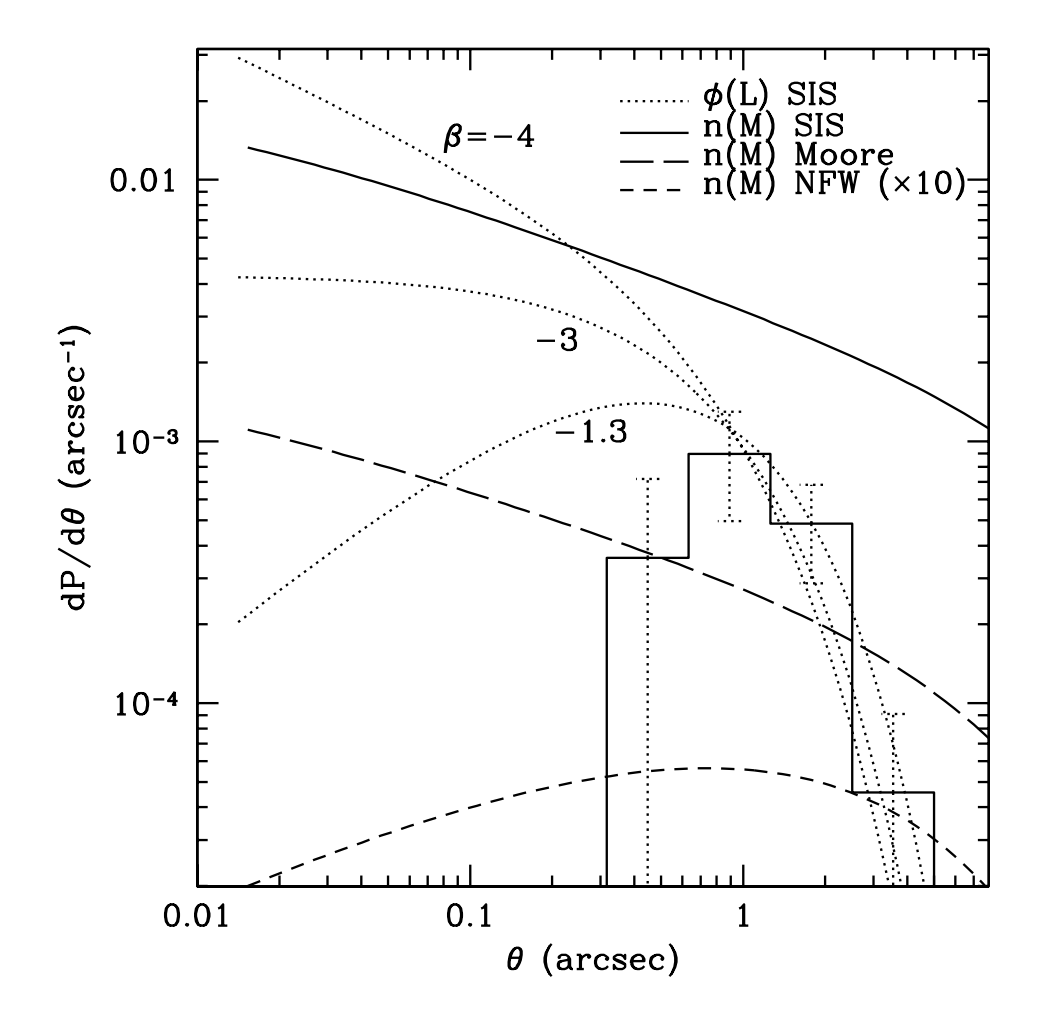


Fig. 2.— Image separation distribution  $dP/d\theta$  calculated from galaxy velocity function (eq. (3); dotted) vs. mass function (eq. (5)). The result depends strongly on the choice of the function and the assumed lens mass profile. The lensing amplitude decreases rapidly as the inner mass profile is lowered from -2 (SIS; solid), to -1.5 (Moore; long-dashed), to -1 (NFW raised by a factor of 10 to fit in the plot; short-dashed). Note that no single halo profile can bring the mass function prediction for  $dP/d\theta$  into agreement with the velocity function prediction. The histogram shows CLASS data as in Fig. 1.

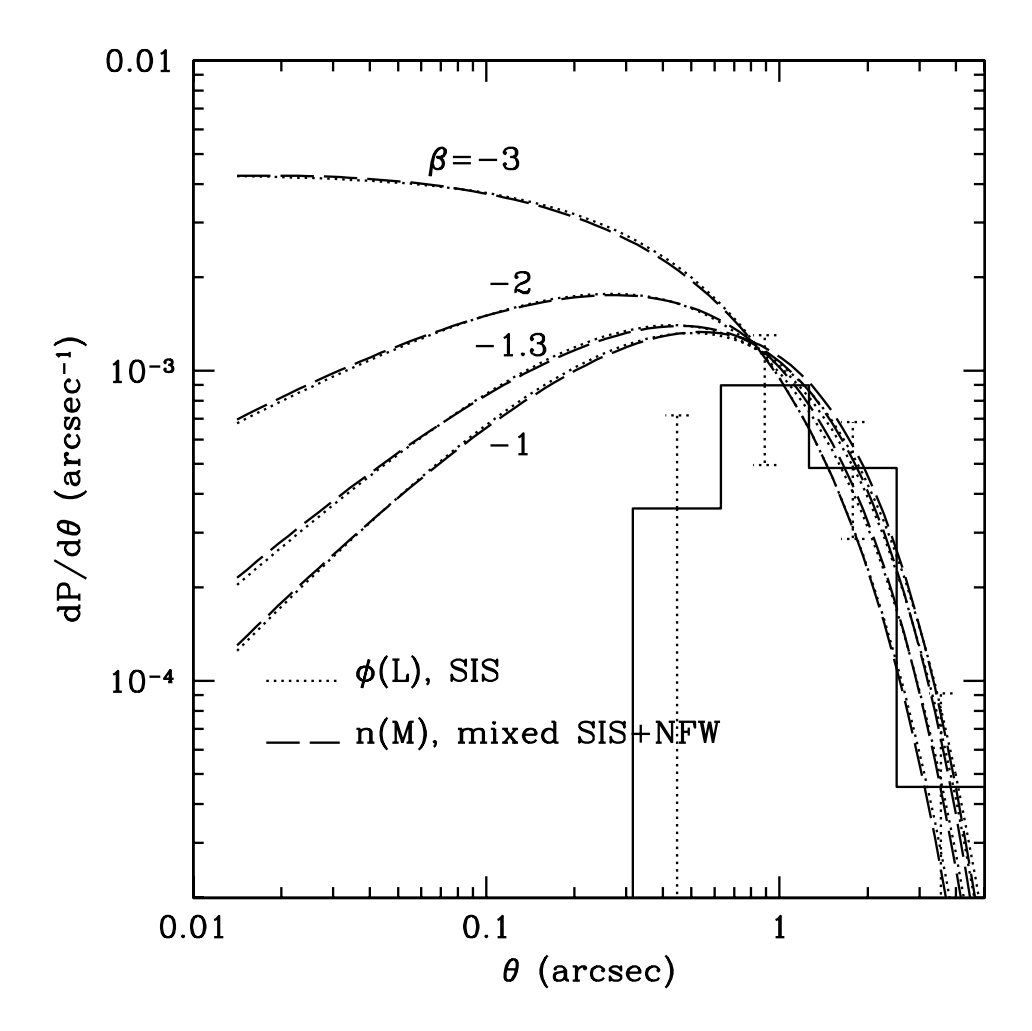


Fig. 3.— Different predictions from velocity vs. mass function in Fig. 2 can be brought into agreement if at a given mass, a fraction  $f_{SIS}(M)$  (eq. (6)) of the dark matter halos is assigned SIS and the rest NFW. The predicted  $dP/d\theta$  from the velocity function (dotted) and the mass function (dashed) then agree very well for suitable choices of parameters  $\eta_1, \eta_2$  and  $M_c$  for  $f_{SIS}$  (see text). The histogram shows CLASS data as in Fig. 1.

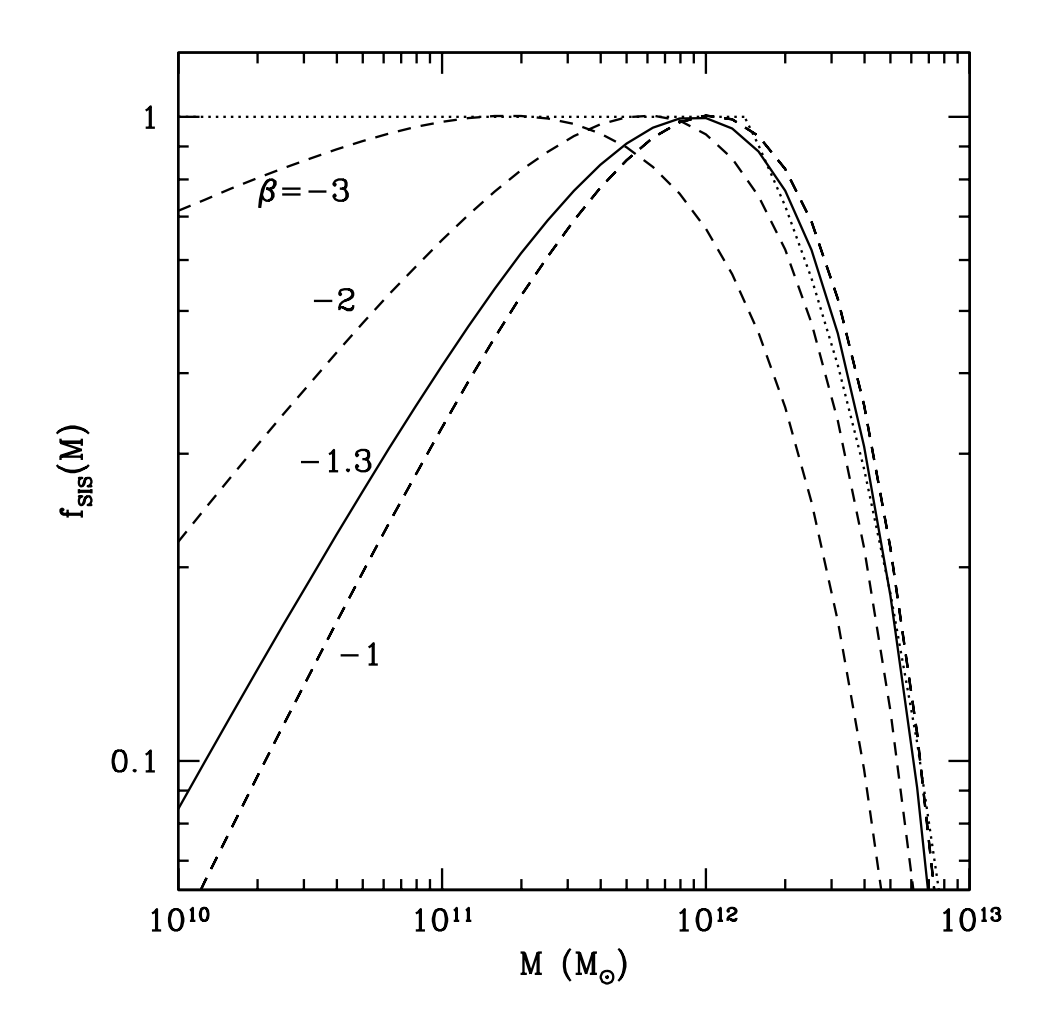


Fig. 4.— The fraction  $f_{SIS}(M)$  of halos with SIS profiles needed for the consistent predictions in Fig. 3. As the faint-end slope  $\beta$  of the velocity function steepens, a larger fraction of low-mass halos is allowed to be SIS. Galaxy surveys favor  $\beta \sim -1.3$  (solid), requiring  $f_{SIS} \sim M^{\eta_1}$  with  $\eta_1 \approx 0.75$  below  $10^{12} M_{\odot}$ . The dotted curve shows Oguri's result (2002), which agrees well with our solid curve at large mass but assumes  $f_{SIS} = 1$  at small mass.